Reprinted from October 1980, Vol. 102, Journal of Mechanical Design

R. D. Flack
Asst. Professor,
Assoc. Mem. ASME

M. E. Leader[1]
Assoc. Mem. ASME

E. J. Gunter
Professor,
Mem. ASME

Department of Mechanical and Aerospace Engineering,
School of Engineering and Applied Science,
University of Virginia,
Charlottesville, Va 22901

An Experimental Investigation on the Response of a Flexible Rotor Mounted in Pressure Dam Bearings

The response of a flexible rotor mounted in six bearing sets has been experimentally determined. One set of axial groove bearings and five sets of pressure dam bearings were tested. Conventional synchronous tracking was used in the analysis and other techniques utilizing an FFT analyzer were developed. The stability of the system was seen to strongly depend on the design of the step bearings. The dam bearings were also noted to lock into subsynchronous whip during deceleration after the system went unstable. The response of the system with varying degrees of unbalance is also analyzed and several structural resonances of the rotor system are discussed.

Introduction

Rotor-fluid film bearing systems are the instigators of many industrial shutdowns. The dynamic behavior of a rotor must be continually monitored such that if its motion or a casing acceleration becomes large the system can be disengaged, hopefully before substantial permanent damage occurs. In many cases the actual cause of a shutdown is sometimes not determined, or if so, only after considerable effort. The typical types of data analysis used by field engineers include synchronous tracking and spectrum analyses. In this paper these and other types of data analysis are performed on a flexible rotor in several sets of fluid film bearings.

Fluid film bearings are used in many applications because of their damping characteristics in rotating machinery. Considerable efforts have been made to theoretically predict response characteristics of rotor/bearing systems and to experimentally examine the characteristics of several types of bearings. One particular bearing type which receives widespread use is the pressure dam (or step) bearing. The operating characteristics of this type of bearing have been recently theoretically examined by Allaire et al., [1] for infinitely long bearings and by Nicholas and Allaire for finite length bearings [2]. Experimentally, the effects of two pressure dam bearings on a flexible rotor system were studied by Leader et al., [3]. Other authors [4-7] have also theoretically examined step bearings. From references [1-3] the dam depth was found to have significant effects on the stability of a rotor/bearing system. A major point of importance from reference [2] was the optimization of the pressure dam bearing for stability. Let the dam depth ratio K' be defined as (see Fig. 1):

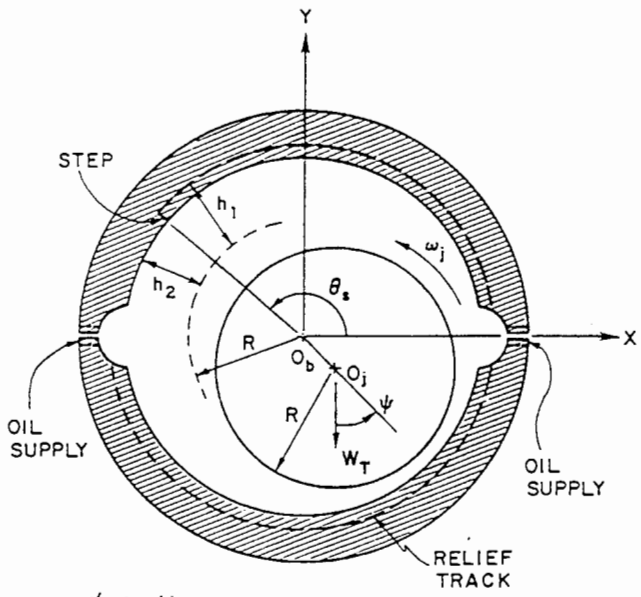

Fig. 1 Pressure dam schematic

$$K' = (h_s + c)/c$$

where

c = bearing clearance
h_s = step height

A theoretically optimum pressure dam bearing has a K' value of approximately 3.0.

[1] Presently, Engineer, Monsanto Chemical Intermediates Co., Texas City, Tex., Assoc. Mem. ASME

Contributed by the Vibrations and Sound Committee for publication in the JOURNAL OF MECHANICAL DESIGN. Manuscript received at ASME Headquarters Nov. 1979.

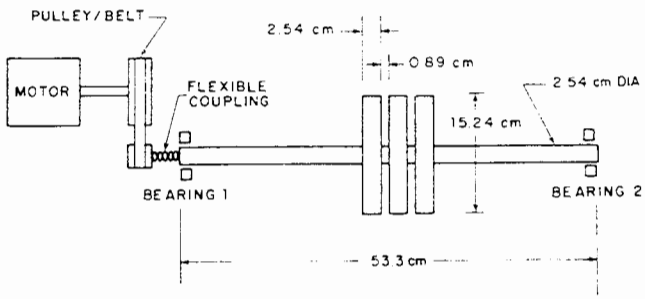

Fig. 2 Shaft and motor assembly

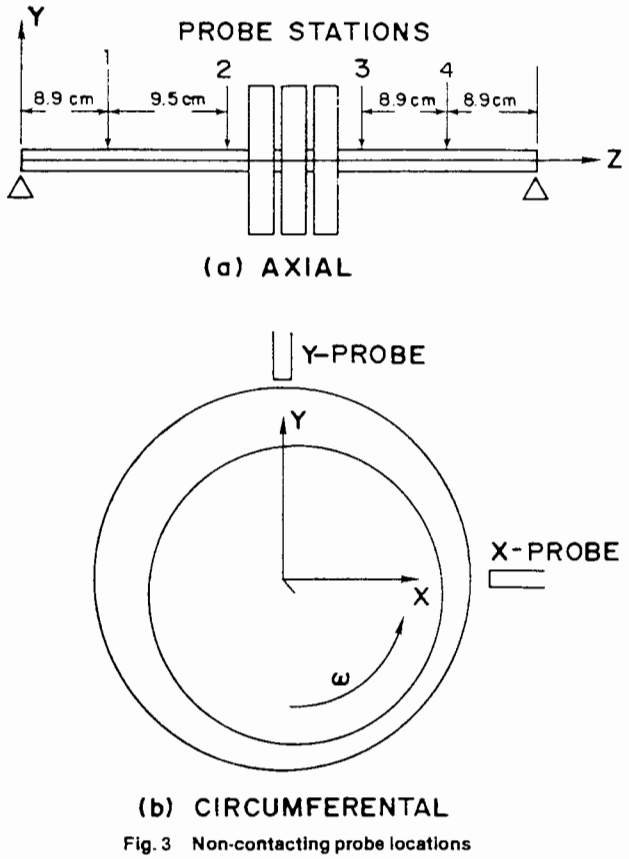

Fig. 3 Non-contacting probe locations

Also, in reference [2] the effect of the circumferential location (θ_s) of the dam was studied. The optimum location was determined to be from 125° to 160° depending upon the Sommerfeld number. In this paper five pressure dam bearings were tested with a flexible rotor; both the values of K' and θ_s were varied.

Overall, very few experimental papers have been available in which flexible rotor-bearing systems have been investigated. The works of Leader et al., [3] and Tonnesen and Lund [8], who studied two-axial groove bearings and squeeze film dampers, represent the major efforts in this area. Most experimental efforts have been directed toward the investigation of only beraing characteristics in which the rotors are essentially rigid.

One type of vibration analysis of rotating machinery which has only received moderate attention is fast Fourier transform (*FFT*) analysis. *FFT* analyzers are capable of much more versatile analyses than real time analyzers or synchronous tracking filters and do in fact complement the latter instruments well.

Thus, the purpose of this paper is to (1) present results for a flexible rotor with pressure dam bearings which were previously not available and (2) to demonstrate some techniques on how conventional and contemporary signal analyzers can be used to analyze rotor systems with several resonance conditions.

The Experimental Apparatus and Procedure

The Test Rig. The test rotor consists of a flexible shaft with three closely mounted disks located midway between two bearing supports (Fig. 2). The combined weight of the shaft and central masses is 13.55 kg. The three masses were mounted onto the shaft by means of a cone and neoprene "O" ring which securely fixed the disks to the shaft without adding any appreciable stiffness. Each disk has 24 balance weight holes each 15° apart. Successive disks were incremented 5° so that a balance hole was available every 5°. The shaft has a constant diameter (2.54 cm) which yields a first critical speed of 3300 rpm. Since the masses were centrally located, higher order, shaft critical speeds were non-existant.

The rotor is driven by a one horsepower DC motor through a flat belt and flexible coupling. A pulley ratio fo 5.65 was used as the maximum speed of the motor was approximately 2250 rpm. The torque and speed of this motor are electronically controlled and operator adjustable. Any rotor speed between 100 and 13,000 rpm can be obtained and held within one rpm. The misalignment of bearings with respect to the shaft is known to effect the response of a rotor-bearing system, particularly for multi-lobe bearings [10]. Thus, the flexible coupling as shown in Fig. 2 was used to minimize this effect.

The interchangeable bearings are mounted in pedestals on top of an oil filled and temperature controlled reservoir. The entire apparatus is clamped to a 900 kg, 0.76 m × 2.13 m × 0.24 m concrete foundation, and the foundation was supported above a concrete floor at the ends and center using rubber dampers.

The oil (Shell automotive type 10W-20W-50) was heated to 54°C (130°F) and fed at low supply pressure (approximately 20.7 KPa) to the bearing surfaces. At this tempertaure the dynamic viscosity was measured to be 50cP (0.75×10^{-5} lb-sec/in^2) with a viscometer. The dynamic viscosity was also 195 and 35.5 cP at 30°C (86°F) and 70°C (158°F), respectively. The right hand bearing has a double thrust bearing included with a clearance of 1.27×10^{-2} cm (5 mils).

For comparison with the pressure dam bearings, a set of two axial groove bearings was also tested. All of the axial groove and step bearings were babbitt lined and did not have end seals. Also, the L/D ratio was approximately unity for these bearings and the two oil grooves were 20° wide. The pressure dam bearings used here did not have relief tracks. The widths of the dams were 1.91 cm. In Table 1, the specifications of the bearings are presented. The ratio, K', as described above is one of the parameters parametrically varied. The circumferential dam location, θ_s, was also varied.

The Instrumentation. Shaft vibrational motion was monitored by eight noncontacting probes mounted in nonmagnetic shells at four locations (Fig. 3). A standard right-hand coordinate system is employed to facilitate comparison to mathematical analysis and computer modeling. The raw signal from a probe was passed through a coaxial cable to an oscillator/demodulator and then to the synchronous tracking filter. Each probe-oscillator/demodulator combination was calibrated for linearity and chosen such that the response of the probes was matched. Thus, direct comparison of the outputs of the various probe was possible. In addition to the vibration pick-ups, a proximity probe was placed over a notch in the shaft on the x-axis as a zero degree reference for balancing and to monitor rotational speed.

The synchronous tracking filter has outputs to display the

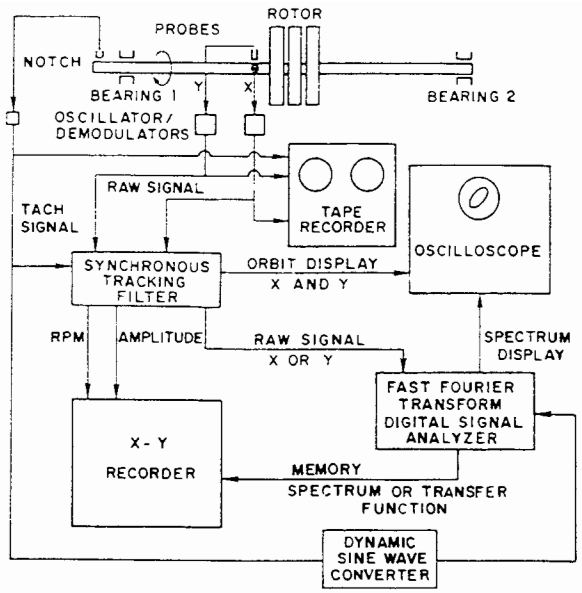

Fig. 4 Block diagram of instrumentation

synchronous and total vibration orbits on the oscilloscope as well as speed and amplitude of vibration outputs for use with the *x-y* recorder (Fig. 4). Phase angle of the synchronous orbit was also plotted against speed. Vibration amplitude was plotted against rpm for each bearing station and for each type of bearing.

Before each test was run, the rotor was balanced at the first critical speed using the three trial weight method. A small residual unbalance resulted from this balance technique for each test. From each synchronous response plot, the unbalance is estimated using the results of Nicholas et al., [9] with the equation

$$\omega_{\min}/\omega_{cr} = (\delta_r/e_u)^{1/2} \tag{2}$$

which applies to a bowed shaft and where:

$\omega_{\min}$ = speed at which the amplitude falls to a minimum on either side of the critical speed
ω_{cr} = observed critical speed
δ_r = bow vector magnitude at the probe location
e_u = unbalance eccentricity

Then the unbalance magnitude is calculated by multiplying e_u by the rotor mass. The shaft had a bow vector of 0.015 mm. The rotor unbalances are included in Table 1. The accuracy range for this method is ± 7 gm-cm.

Two test runs were made for each bearing. For the first the speed of the rotor was increased at maximum acceleration up until the stability threshold was reached, at which point the power was shut off and the rotor was allowed to coast to a stop. The average acceleration rate was 15 rad/sec^2 and the average deceleration rate was −8 rad/sec^2. For the second test, the speed of the rotor was increased at a very low acceleration rate (typically 2 rad/sec^2) until the stability threshold was again reached. During the tests the motion and speed of the rotor were carefully monitored by using the synchronous tracking filter. The data was also recorded by a fourteen channel FM tape recorder such that the data could be further analyzed after the tests.

After the tests were run, data was reduced by three methods. First, both the synchronous and total (synchronous plus nonsynchronous) amplitudes of the motion at the various locations were plotted as a function of the rotor speed using the data from the first test. The phase of the synchronous motion was also plotted.

Also from the first test, a transfer function of the system was found. To obtain this, the output of the proximity probe used to monitor the shaft notch was input into a dynamic sine wave converter to convert the once per revolution pulse into a constant amplitude sine wave with the frequency of the shaft speed. The frequency of this sine wave, thus, approximated the forcing frequency representing the rotor unbalance. Using a fast Fourier transform digital signal analyzer and using the signal of any one of the proximity probes as the output variable and the sine wave described above as the input variable, a transfer function was determined. This transfer function was plotted versus rotor speed and is compared to the output of the synchronous tracking filter and also plotted in Nyquist form. The amplitude of this data is in relative form.

From the second set of recorded data "cascade" or "waterfall" plots were constructed. A fast Fourier transform digital signal analyzer was used to obtain frequency spectrums during the slow accelerations. One data sample was collected and analyzed in speed increments (typically 500 rpm). By plotting the spectrums vertically the "waterfall" plots were obtained. Also, it was found that if the acceleration rate was low (2 rad/sec^2), by using one sample at each speed, spectrums were obtained which were identical to those obtained at constant speed plateaus using 200 to 400 samples. The instrumentation used in this study is summarized in Fig. 4.

Lastly, during the tests described above several resonances were observed using the proximity probes. Several of these were determined to be structural resonances by supplementary impact tests. The purpose of these tests was to determine the causes of the resonances and not necessarily the damping or amplification factor of each resonance. To impart an impulse, a rubber mallet was used on the rotor structure (motor casing, bearing pedestals, etc.), while a 50 pound sandbag was dropped onto the concrete foundation. Thus, the actual magnitudes of the impulses were unknown. A velocity transducer was mounted on various portions of the structure for different tests and the output of the transducer was analyzed with the *FFT* analyzer. For these tests auto power spectrums (with peak hold) were used. Although the actual magnitudes of the peak frequency responses are not known the relative peaks and the coresponding frequency were readily observable. Also, the frequencies at which the resonances occurred were found not to be functions of the amplitude of the impulse force, which was expected. Thus, using these impact tests probable causes of the resonances were determined.

Experimental Results

The two aims of the experimental program were to experimentally examine the response of the rotor-bearing systems when it was under acceleration and at different speeds and to investigate the response of the system at the onset of instability. The experimental apparatus was instrumented with eight noncontacting probes as described earlier. Only representative results are presented here.

Two-Axial Groove Bearings. These bearings are the simplist deviation from a plain circular journal bearing, having two grooves in a horizontal plane to admit lubricant. The response of the rotor with this bearing will be considered a standard against which the response of the rotor with pressure dam bearings will be compared.

The test rotor was relatively easy to balance with the axial groove bearings by cancelling the residual bow at the first rotor critical speed. This can be seen by examining Fig. 5 in which the bearing end vertical shaft motion (Y 1) for rotor acceleration (run-up) is plotted. On this figure both the synchronous and total motions and the relative phase angle (as measured from the shaft notch) are presented. One can see

Table 1 Pressure dam bearing specifications

BEARING TYPE	BEARING NUMBER	INSTALLED RADIAL CLEARANCE c (mm)	STEP HEIGHT h_s (mm)	K* RATIO $(h_s + c)/c$	STEP LOCATION (θ_s^-).	L/D RATIO	ROTOR UNBALANCE (gm-cm)
2 AXIAL GROOVE	1	0.046	N.A.	N.A.	N.A	1.0	22
	2	0.051	N.A.	N.A.			
PRESSURE DAM SET #1	1	0.056	0.064	2.1	145°	1.0	22
	2	0.064	0.091	2.4			
PRESSURE DAM SET #2	1	0.064	0.112	2.8	140°	1.0	20
	2	0.064	0.104	2.6			
PRESSURE DAM SET #3	1	0.061	0.340	6.6	150°	1.0	23
	2	0.064	0.483	8.6			
PRESSURE DAM SET #4	1	0.061	0.140	3.3	90°	1.0	20
	2	0.061	0.069	2.1			
PRESSURE DAM SET #5	1	0.053	0.569	11.7	140°	1.0	20
	2	0.061	0.442	8.3			

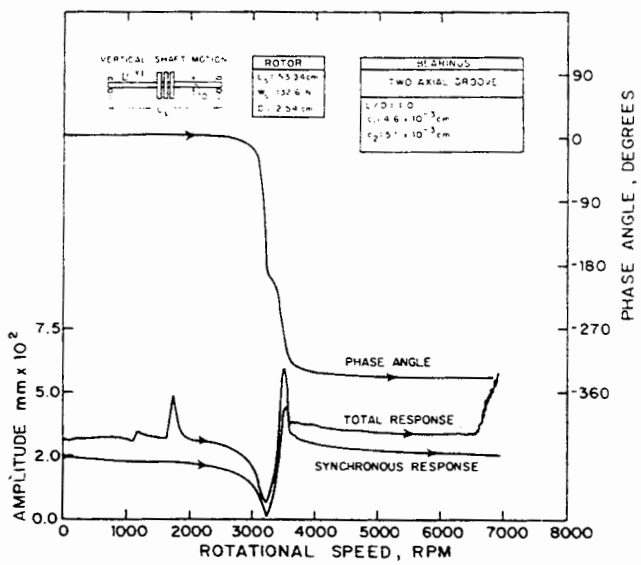

Fig. 5 Y1 synchronous and total motion, axial groove bearings

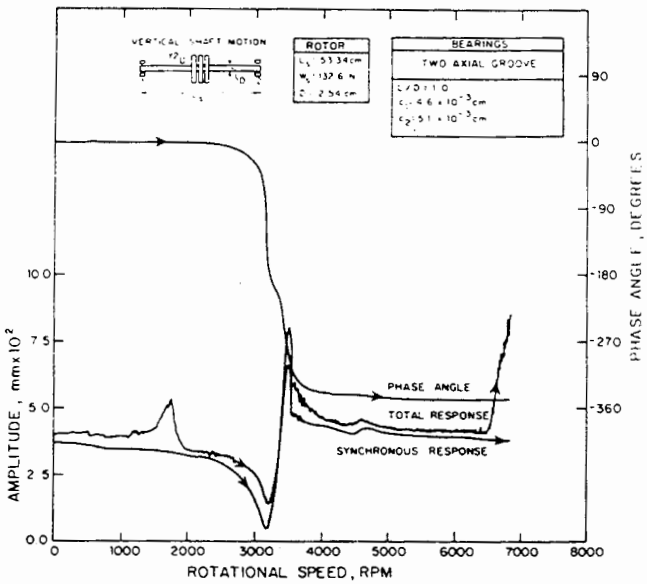

Fig. 6 Y2 synchronous and total motion, axial groove bearings

that at the first critical speed (3250 RPM) the bow vector is removed since the synchronous response drops to approximately zero at this speed.

For comparison, the motions at two other locations (Y 2 and X 2) are presented in Figs. 6 and 7. Overall the shapes of three curves are very similar. The actual magnitudes are, of course, somewhat different. The total motion of the central vertical plane (Y 2) is 0.084 mm as compared to 0.050 mm in the Y1 plane at 3400 RPM. The amplitude near the center of the rotor should be expected to be larger near the first critical. The motion in the X 2 plane is 0.048 mm.

As the rotor increases in speed the stability threshold is reached at 6600 rpm, approximately twice the first critical speed. This threshold is evidenced by a rapid increase in the total motion response of the rotor. The maximum total amplitudes seen at Y 1, Y 2 and X 2 are 0.058, 0.089 and 0.086 mm, respectively. At the instability condition the amplitude of the synchronous component is seen to be constant.

Other responses are noted in the rotor motion in Figs. 5 to 7 and these occur at approximately 1600 rpm and 4600 rpm. The first is a supersynchronous excitation of the rotor first critical and the second in synchronous excitation of a structural resonance. These resonances and others will be investigated and discussed later.

The synchronous phase angle is seen to shift by 360 deg at the critical speed for Y 1, Y 2, and X 2, which does not conform to the ideal 180 deg shift at a resonance. This behavior is due to the initial shaft bow. A small shift in phase is also seen at 4600 rpm. These phase shifts will be discussed in more detail with the pressure dam bearings.

To complement the synchronous tracking filter data the *FFT* analyzer was used to produce cascade plots for the rotor run up (position X 2) and is presented in Fig. 8. The synchronous component can easily be seen on this waterfall plot and compared to Fig. 7. For example, a maximum is seen at 3500 rpm and minimums are seen at 3100 rpm and 4600 rpm

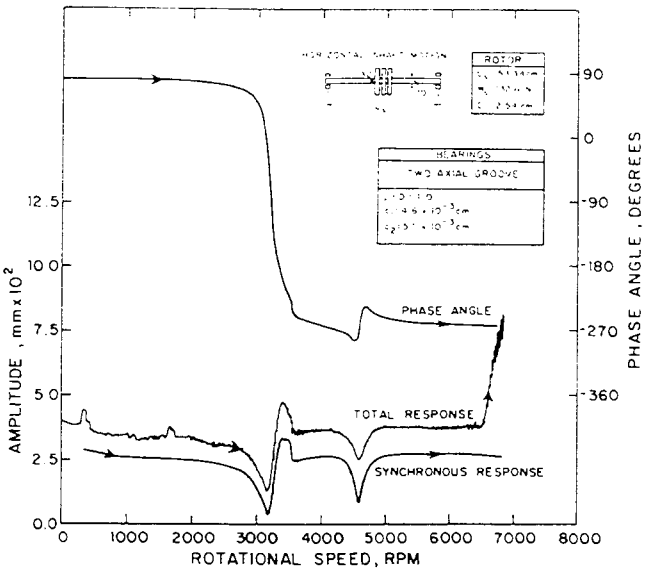

Fig. 7 X2 synchronous and total motion, axial groove bearings

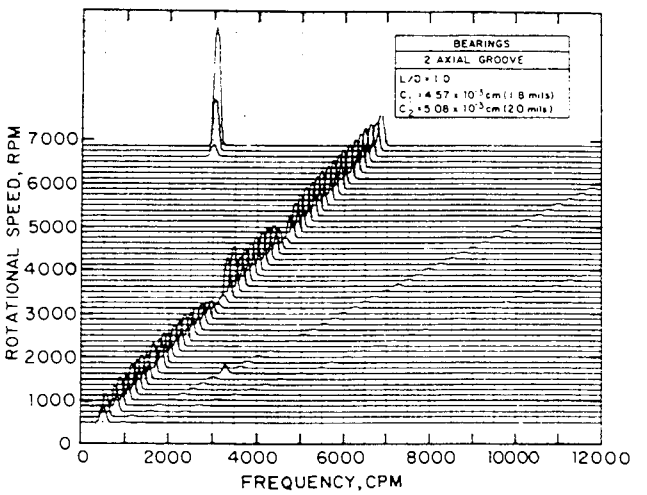

Fig. 8 X2 motion cascade plot, axial groove bearings

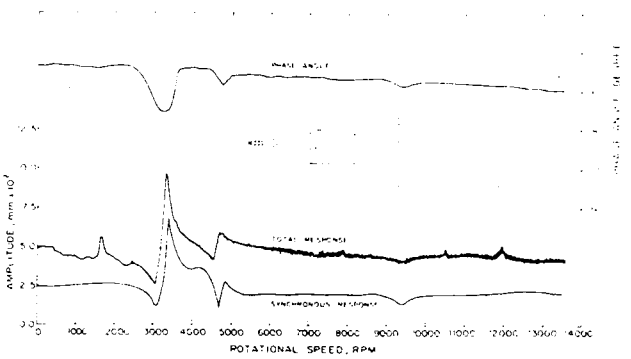

Fig. 9 X2 synchronous and total motion, pressure dam set #1

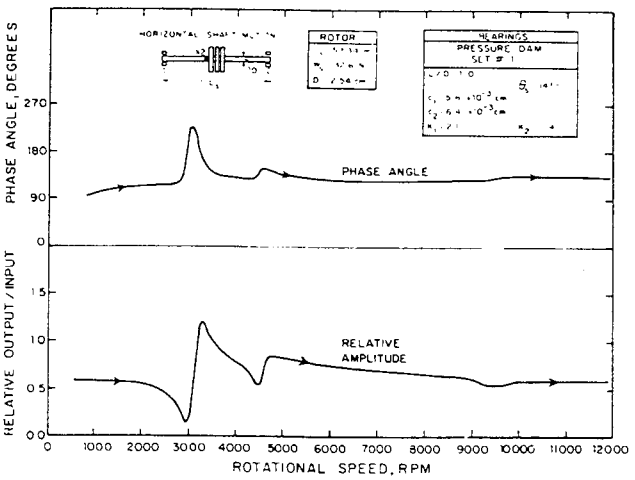

Fig. 10 Transfer function (X2 motion = output, rotor unbalance = input) pressure dam set #1

on both Figs. 7 and 8. At the instability condition (6600 rpm) a large subsynchronous component at 3100 cpm is seen while the amplitude of the synchronous component remains at the pre-instability value.

Also on Fig. 8 the frequency components at two and three times running speed can be seen. Particularly, at 1650 rpm a relatively large component is seen at 3300 cpm (approximately the rotor first critical speed), while the synchronous component remained constant at this speed. This observation agrees with the peaks for the total motion seen at 1600 rpm in Figs. 5 to 7.

In Figs. 5 to 8 data was presented for the rotor run-up. For run down the data was almost identical and is not presented here for brevity. For the pressure dam bearing data this was not the case and one typical run down plot will be presented.

Pressure Dam Bearings. The rotor was run with five different pressure dam bearings as described in the previous section. The first data presented here is for set number 1 which had K' ratios of 2.1 and 2.4.

In Fig. 9 the X 2 total and synchronous motion is presented for rotor run-up. The critical speed was relatively unchanged from that of the rotor with the axial groove bearings. This rotor system also displays the resonance responses at 1600 rpm, 3300 rpm and 4600 rpm and also a synchronous response at 9400 rpm. This system accelerated until the maximum speed of the rotor was reached, namely 13,500 and never reached the stability limit. The synchronous phase displayed a change at the critical speed but did not shift by 180 deg as the critical speed was traversed. The net phase shift was zero.

To better understand this and the axial groove bearing phase shift phenomena and to investigate the capabilities of an *FFT* analyzer the transfer function was found for the X 2 motion for this case. The procedure for this analysis was described earlier. The reduced data is presented in Fig. 10. This plot very closely represents the synchronous tracking filter plot of Fig. 9. Again, three synchronous resonances are seen: 3300 rpm, 4600 rpm and 9500 rpm. Synchronous phase shifts are also almost indentical to those observed with the synchronous tracking filter (although inverted due to the different definitions of phase angle of the manufacturers of the synchronous tracking filter and *FFT* analyzer).

In Fig. 11 the Nyquist form of the transfer function is presented. On this plot several running speeds are denoted such that comparisons to Fig. 10 can be made. In Fig. 11, the vector representing the initial bow, δ_r, is included. For this data one can easily see why the classical 180-deg phase shift was not observed at the first critical speed: the center of the Nyquist plot was located outside of the Nyquist loop representing the first critical speed due to the initial bow vector. A net phase shift of approximately 0 deg was thus observed. Had the center fallen on the loop ($\delta_r = 0$) the classical 180-deg phase shift would have been observed. If the center had fallen inside the loop, a 360-deg phase shift would have been observed. The latter case was seen for the shaft with the axial groove bearings (Figs. 5 to 7).

This behavior is best understood by using the theoretical method developed in reference [9]. When the bow and un-

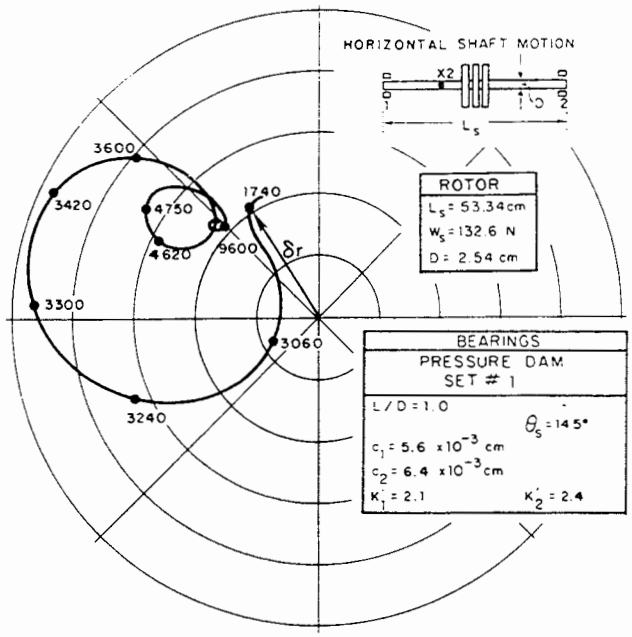

Fig. 11 Transfer function - Nyquist form (X2 motion), pressure dam set #1

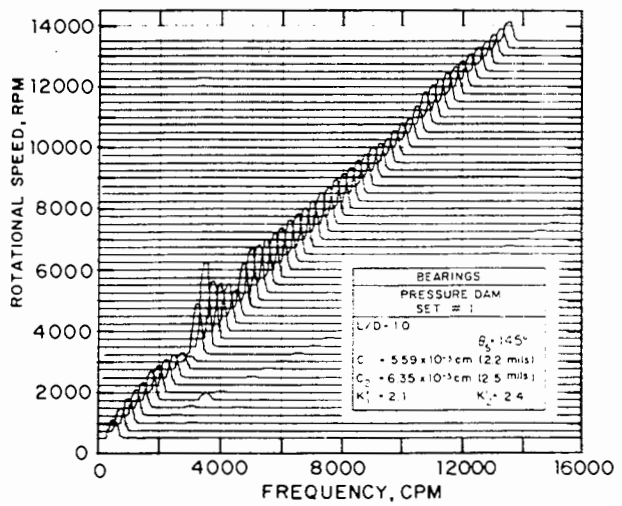

Fig. 12 X2 motion cascade plot, pressure dam set #1

balance vectors are of equal magnitude and when they are 180 deg out of phase, a sudden 180-deg phase shift is observed at the critical speed. However, when they are, say, 179 or 181 deg out of phase, net 0 and 360 deg phase shifts, respectively, are seen. Thus, the placement of the balance weight strongly affects the phase response when a rotor is balanced near a critical speed.

Also in Fig. 11 two smaller loops are seen. These occur at approximately 4600 rpm and 9500 rpm and represent the responses seen in Figs. 9 and 10. These resonances are structural modes and will be discussed later.

Next, the X 2 waterfall plot for pressure dam set 1 is presented in Fig. 12. On this plot only the synchronous and twice synchronous frequency components are readily noticeable while a third order component is slightly visible. No subsynchronous components are evident. Particularly, at high rotational speeds this cascade plot shows the rotor system to be highly stable since a subsynchronous component at the rotor first critical speed is not evident.

Other probe signals were analyzed as above. No significant differences were observed, however. For example, the X 1 data was similar to the X 2 data except that the amplitude was

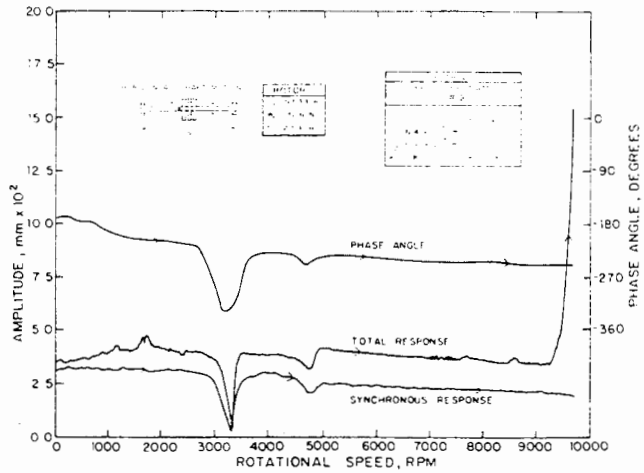

Fig. 13 X2 synchronous and total motion, pressure dam set #2, run-up

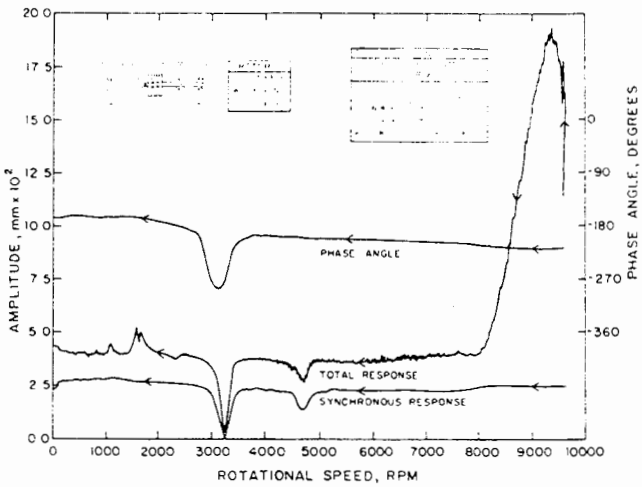

Fig. 14 X2 synchronous and total motion, pressure dam set #2, run-down

less at all speeds. No strong resonances were observed in the X1 data that were not observed in the X2 data and vice versa.

Data from pressure dam set number 2 (X 2 motion) is presented in Fig. 13 for run-up and Fig. 14 for run-down. This data is similar to the axial groove and pressure dam set 1 data since similar synchronous and total motion resonances are noticed at 3300 rpm and 4700 rpm, and 1700 rpm, respectively. Upon run-up the rotor with these bearings reaches a stability limit at 9300 rpm (Fig. 13). On a waterfall plot (not presented) this instability was seen to excite the first rotor critical speed. Upon deceleration (Fig. 14) the motion of the rotor is seen to differ from that on run-up. The rotor locks into the subsynchronous motion and continues until the speed decreases to 8100 rpm. The speed range for which the rotor locks into this whip condition will be referred to as N_w and is equal to 1200 rpm for this case. For speeds lower than 8000 rpm the deceleration and acceleration responses are nearly identical.

Three other pressure dam bearings were tested and graphical results are not presented here for brevity. All of the pressure dam bearings exhibited similar characteristics. Particularly, resonances were always seen at approximately 1600 rpm, 3300 rpm and 4600 rpm. Also, when the rotor went unstable the dominating frequency component occurred at 3300 rpm, the first rotor critical speed. Also, for all of the tests the rotor locked into the subsynchronous whip on deceleration. It was found that the value of N_w increased with increasing instability threshold. This observation is noted here, but enough data was not obtained to determine or generalize this relationship for pressure dam bearings. Also,

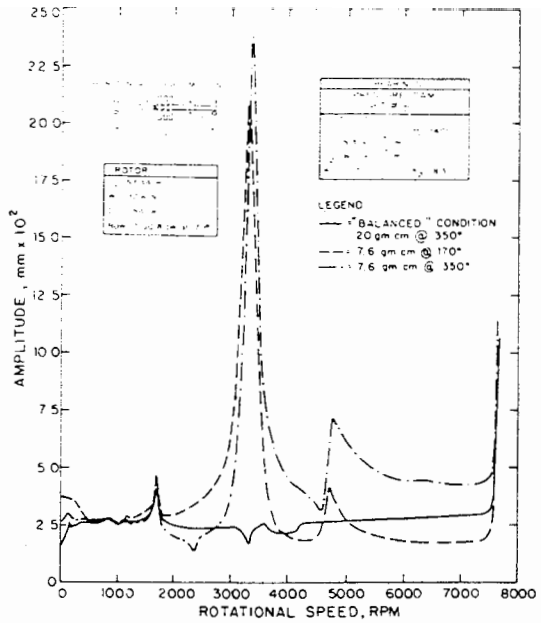

Fig. 15 X2 total motion for varying degrees of unbalance, pressure dam set #5

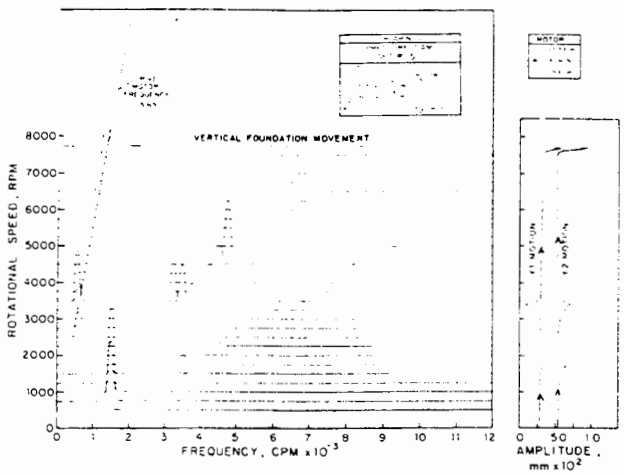

Fig. 16 Vertical foundation motion cascade plot, pressure dam set #5

Nicholas et al., [11] have predicted the instability thresholds of axial groove and pressure dam bearings as studied here. Agreement between the predictions and experimental data is generally within 20 percent.

Rotor Unbalance. In all of the previously discussed results the rotor was balanced such that the bow vector was cancelled at the first rotor critical speed. Tonnesen and Lund [8] found that adding rotor unbalance reduced the instability threshold speed of a rotor for axial groove bearings. To examine such characteristics of the present rotor system, four supplementary tests were run for the rotor in pressure dam set number 5. The rotor unbalance was varied by placing known masses in the balance holes of the rotor. For these runs the bow of the rotor was 0.018 mm and unbalances of 4.6 gm-cm and 7.6 gm-cm were placed in the central mass in phase and 180° out of phase with the rotor bow.

Typical results are presented in Fig. 15. In this figure the total X 2 motion is plotted vs rotor speed for three values of unbalance. As can be seen the instability threshold is unaffected by the unbalances used here. Using larger unbalances was not possible without risking damage to the rotor system. The major differences of the responses occur at 3300 rpm and at 4600 rpm which were system resonances as indicated earlier. The largest responses are seen for the cases when the

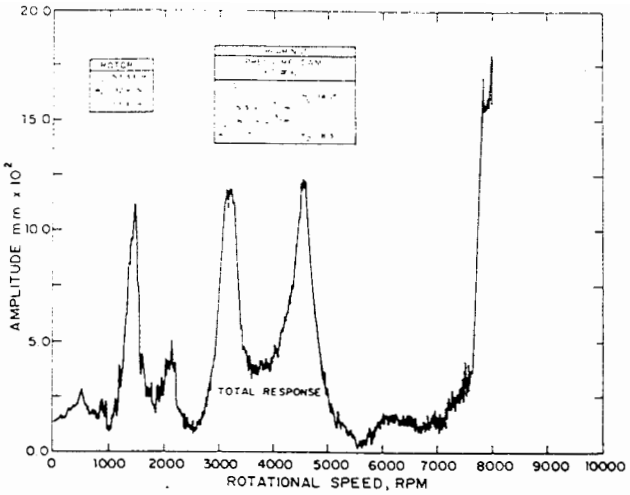

Fig. 17 Vertical foundation total motion, pressure dam set #5

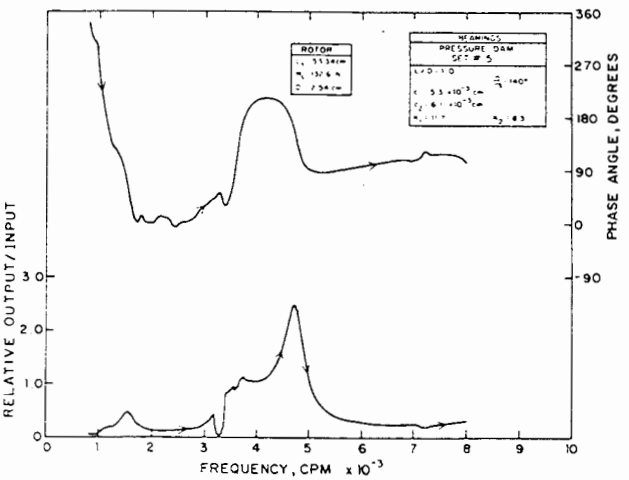

Fig. 18 Transfer function (vertical foundation motion = output, Y2 shaft motion - input), pressure dam set #5

Table 2 Vertical foundation motion peak responses

FREQUENCY (CPM)	AMPLITUDE (mm x10²)
500	3.0
1500	12.0
2160	5.0
3250	14.0
4650	15.0

unbalance is 180 deg out of phase with the rotor bow. Tests with 4.6 gm-cm are similar except that the amplitudes are less.

Structural Resonances. On most of the synchronous motion plots already presented, resonances were seen at 4600 rpm and 9400 rpm. To identify these resonances a series of tests were performed: (1) the vertical motion at the center of the concrete block was measured as a function of rotor speed, (2) a velocity transducer was used to measure the response of various sections of the foundation and rotor support to impulse forces imparted to other sections of the structure. This data was collected when the rotor was mounted in pressure dam bearing set number 5. For the impact tests the installation of different bearing sets had no effect.

Typical data for the first part of these tests is presented in Figs. 16 to 18. In Fig. 16 the total amplitude of the shaft vertical motion is presented for reference. From this plot several phenomena are observed. Firstly, between the rotor speeds of 3000 rpm and 5000 rpm significant motion at the

Table 3 Summary of impact tests

IMPACT IMPARTED TO/RESPONSE MEASURED ON	FREQUENCIES OBSERVED (CPM)				
Vertical Foundation/Vertical Foundation		1500*			
Vertical Foundation/Vertical Pedestal	500	1500*	2000		
Vertical Pedestal/Vertical Foundation		1500*			8750
Horizontal Foundation/Horizontal Motor	500*	1300		4750	
Vertical Foundation/Horizontal Motor	500			4750*	
Horizontal Foundation/Vertical Pedestal	300	1500*	1950	4750	8750
Vertical Pedestal #2/Vertical Pedestal #1	500	1500	2000*		

* Predominate Frequencies

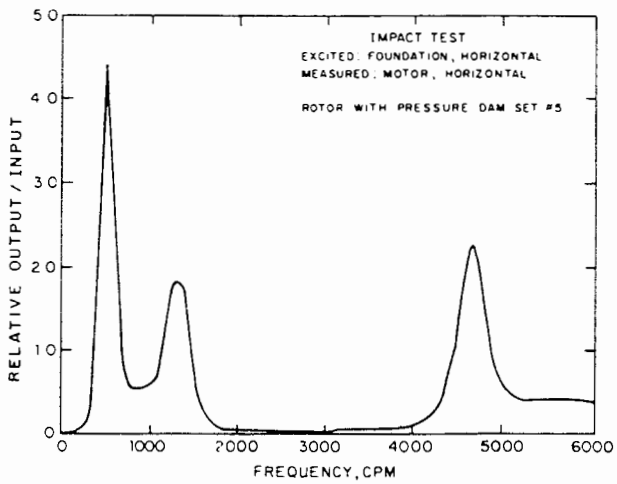

Fig. 19 Structural impact test, horizontal motor response to horizontal foundation excitation

Table 4 Structural resources

APPROXIMATE FREQUENCY (CPM)	PROBABLE CAUSE
500	Concrete Block Horizontal Motion
1500	Concrete Block Vertical Motion
2000	Bearing Pedestal Motion
4750	Cantilever Motor Horizontal Motion
8750	Rotor Mounting to Concrete Block

rotor frequency is observed. Secondly, a significant component at 18 percent (1/5.65) of the rotor speed is usually observed. These frequencies are attributed to the fact that the motor/rotor rotational speed is 1:5.65. Lastly, a significant response at a frequency of 1500 cpm is observed when the rotor frequency is 750 rpm.

The total vertical motion as a function of rotor speed is presented in Fig. 17. Several peaks are observed and these frequencies and their amplitudes are summarized in Table 2.

In Fig. 18 the transfer function (vertical foundation motion/vertical shaft motion, Y2) is presented. This was obtained with the *FFT* analyzer. This plot tends to remove the first rotor critical speed from the response curve since the structure is actually responding to the rotor unbalance or shaft motion of the rotor system. As can be seen a strong resonance occurred at 4700 rpm.

To explain the various resonances a series of impact tests were performed as described earlier on the rotor system and the responses of the transducers were analyzed. For example, the output for the horizontal motor casing response to a horizontal foundation excitation is presented in Fig. 19. Large resonances are seen at 500 cpm, 1300 cpm and 4700 cpm. Similar frequency spectrums for other locations and tests were performed and significant results are summarized in Table 3. By using the results in Table 3 the probable causes of the five structural resonances have been determined. These are listed in Table 4.

Summary

The response of a simple flexible rotor has been investigated for a set of axial groove bearings and five sets of pressure dam bearings. A synchronous tracking filter and an *FFT* analyzer were utilized to analyze the outputs form shaft monitoring proximity probes and from a velocity transducer monitoring structural resonances. Specific conclusions from the study include: (1) the optimum value of K' for the step bearings was seen to be 2.1/2.4 and experimental results were seen to compare well with other theoretical results, (2) the rotor with pressure dam bearings locked onto subsynchronous whip on run down and the length of time it remained in whip increased as the stability threshold increased, (3) the *FFT* analyzer was found to be much more valuable than for simply obtaining spectrums, and a *FFT* transfer function technique was developed for obtaining an analysis similar to synchronous tracking, (4) by plotting this transfer function in a Nyquist form the effects of rotor bow can be easily analyzed, (5) adding large amounts of rotor unbalance was seen not to affect the stability threshold for one bearing set, and (6) structural resonances were observed at 500 cpm, 1500 cpm, 2000 cpm, 4750 cpm and 8750 cpm and the probable causes were identified by using a synchronous tracking filter and a *FFT* transfer function and spectrum analysis.

Acknowledgment

The authors wish to thank Drs. J. C. Nicholas, L. E. Barrett, P. E. Allaire and D. W. Lewis for their helpful discussions during this investigation. This research was sponsored by the Department of Energy under contract EF-76-5-01-2479 and the Industrial Supported Program for the Dynamic Analysis of Turbomachinery at the University of Virginia.

References

1 Allaire, P. E., Nicholas, J. C., and Barrett, L. E., "Analysis of Step Journal Bearings - Infinite Length, Inertial Effects," ASLE Preprint, No. 78-AM-3B-1.

2 Nicholas, J. C., and Allaire, P. E., "Analysis of Step Journal Bearings - Finite Length Stability," ASLE Preprint No. 78-LC-6B-2.

3 Leader, M. E., Flack, R. D., and Allaire, P. E., "Experimental Study of Three Journal Bearings with a Flexible Rotor," ASLE Preprint No. 79-AM-6D-2.

4 Wilcock, D. F., and Booser, E. R., *Bearing Design and Application*,

McGraw-Hill, New York, 1957.

5 Pinkus, O., and Sternlicht, B., *Theory of Hydrodynamic Lubrication*, McGraw-Hill Book Company, New York, 1961.

6 Kettleborough, C. F., "An Approximate Analytical Solution for the Stepped Bearing," ASME, *Journal of Applied Mechanics*, Vol. 83, 1961, pp. 507-510.

7 Hamrock, B. J., and Anderson, W. J., "Rayleigh Step Journal Bearing, Part II - Incompressible Fluid," ASME, *Journal of Lubrication Technology*, Vol. 90, 1969, pp. 641-650.

8 Tonnesen, J., and Lund, J. W., "Some Experiments on Instability of Rotors Supported in Fluid Film Bearings," ASME, *Journal of Mechanical Design*, Vol. 100, No. 1, Jan. 1978, pp. 147-155.

9 Nicholas, J. C., Gunter, E. J., and Allaire, P. E., "Effect of Residual Bow on Unbalance Response and Balancing of a Single Mass Flexible Rotor, Part 1: Unbalance Response," ASME, *Journal of Engineering for Power*, Vol. 98, No. 2, Apr. 1976, pp. 171-181.

10 Tondl, A., *Some Problems of Rotor Dynamics*, Publishing House of the Czechoslovak Academy of Sciences, Prague, 1965.

11 Nicholas, J. C., Barrett, L. E., and Leader, M. E., "Experimental-Theoretical Comparison of Instability Onset Speeds for a Three Mass Rotor Supported by Step Journal Bearings," ASME, *Journal of Mechanical Design*, Preprint No. 79-DET-56.